*remote sensing*

MDPI

*Article*

# Four Decades of Thermal Monitoring in a Tropical Urban Reservoir Using Remote Sensing: Trends, Climatic and External Drivers of Surface Water Warming in Lake Paranoá, Brazil

**Alice Rocha Pereira [1,*], Rejane Ennes Cicerelli [2], Andréia de Almeida [3], Tati de Almeida [2] and Sergio Koide [1]**

[1] Departamento de Engenharia Civil e Ambiental, Universidade de Brasília, Brasilia 70910-900, DF, Brazil; skoide@unb.br
[2] Instituto de Geociências, Universidade de Brasília, Brasilia 70910-900, DF, Brazil; rejaneig@unb.br (R.E.C.); tati_almeida@unb.br (T.d.A.)
[3] Faculdade UnB Planaltina, Universidade de Brasília, Brasilia 73345-010, DF, Brazil; andreia.almeida@unb.br
* Correspondence: alice_rp@hotmail.com

## Highlights

**What are the main findings?**

- Remote sensing revealed spatial and seasonal heterogeneity in lake surface warming.
- Air temperature, solar radiation, humidity, and wind speed are the main external drivers.

**What is the implication of the main finding?**

- In situ and satellite-derived water surface temperatures reveal climate-driven lake warming.
- Findings support hydrodynamic modeling and water quality management in urban tropical reservoirs.

## Abstract

This study analyzed how external forcings, such as meteorological conditions and inflows, influence the average water surface temperature (WST) of the urban Lake Paranoá, Brasília-Brazil, using both in situ measurements and remote sensing estimates over a 40-year period. The temperature model calibrated for Lake Paranoá with no time lag (0-day delay) presented the following metrics: $R^2$ = 0.92, RMSE = 0.59 °C, demonstrating the feasibility of obtaining reliable thermal estimates from remote sensing even in urban water bodies. Simple and multiple regression analyses were applied to identify the main external drivers of WST across different temporal scales. A warming trend of 0.036 °C/yr in lake surface temperature was observed, higher than the concurrent increase in air temperature (0.026 °C/yr), suggesting enhanced thermal stratification that may impact water quality. The most influential variables on WST were air temperature, relative humidity, and wind speed, with varying degrees of influence depending on the time scale considered (daily, monthly, annual or seasonal). Remote sensing proved to be essential for overcoming the limitations of traditional monitoring, such as temporal gaps and limited spatial coverage, and allowed detailed mapping of thermal patterns throughout the lake. Integrating these data into hydrodynamic models enhances their diagnostic, predictive, and decision-support capabilities in the context of climate change.

**Keywords:** water surface temperature; lake; Landsat; external forcings; Google Earth Engine



Academic Editors: Gabriel Senay, Deepak R. Mishra, Ge Sun, Yun Yang and Ning Liu

Received: 10 July 2025
Revised: 24 September 2025
Accepted: 16 October 2025
Published: 31 October 2025

**Citation:** Pereira, A.R.; Cicerelli, R.E.; de Almeida, A.; de Almeida, T.; Koide, S. Four Decades of Thermal Monitoring in a Tropical Urban Reservoir Using Remote Sensing: Trends, Climatic and External Drivers of Surface Water Warming in Lake Paranoá, Brazil. *Remote Sens.* **2025**, *17*, 3603. https://doi.org/10.3390/rs17213603

## 1. Introduction

Lakes play a crucial role in the global water cycle and act as sensitive indicators of climate variability and change. Recent studies have documented significant warming trends in inland waters across diverse climatic regions, with rates ranging from 0.01 °C to 0.08 °C per year [1–6]. Among the key physical parameters governing lake dynamics, water surface temperature (WST) is particularly important, as it directly controls thermal stratification, biogeochemical processes, and overall water quality [1,5,7]. Long-term variations in temperature have been increasingly associated with climate change, affecting aquatic ecosystems, ecosystem services, and water resource availability worldwide [1,5,7,8].

The dynamics and consequent spatiotemporal distribution of temperature in lakes are the result of complex interactions of external forces—solar radiation, air temperature, relative humidity, wind, precipitation, evaporation, inflows, and outflows [5,7,9–11]. These factors control energy exchanges at the air–water interface and determine the timing and intensity of stratification and mixing events, shaping nutrient cycling, oxygen dynamics, chlorophyll distribution, and the occurrence of harmful algal blooms [12]. When stratification persists, hypolimnetic anoxia can develop, triggering anaerobic processes and the release of toxic compounds such as ammonia and hydrogen sulfide, as well as resuspension of sediments at the thermocline [13–15]. Conversely, destratification promotes vertical mixing, which may also resuspend bottom material and release nutrients, fueling eutrophication and algal proliferation [14].

Monitoring these processes is challenging because in situ sampling provides limited spatial and temporal resolution. In this context, satellite remote sensing has emerged as a powerful and cost-effective alternative for assessing WST, complementing conventional measurements [12,16–18]. Over the last two decades, thermal remote sensing has enabled continuous, spatially distributed WST monitoring across different climatic settings [12,19]. Platforms such as Google Earth Engine (GEE) enhance the capacity to process long-term and large-scale datasets, supporting analyses of seasonal cycles, warming trends, and extreme events in lakes, including those in tropical and urban environments [6,20–22].

Among the existing thermal sensors, the Landsat series is notable for combining 100–120 m TIR spatial resolution with multi-decadal continuity and global free access, making it well suited for capturing spatial heterogeneity inside lakes and long-term WST monitoring in small to medium lakes [5,19,23]. Studies using GEE and Landsat data have revealed consistent WST increases worldwide in response to climate change, with direct implications for circulation, oxygen solubility, eutrophication, and ecosystem resilience [24–27].

Lake Paranoá is an urban reservoir in Brasília (Brazil) of high landscape and socioeconomic value. Its catchment is highly urbanized; the lake supplies drinking water and supports multiple uses, including wastewater dilution, fisheries, navigation, and hydropower. The system has experienced episodes of eutrophication and cyanobacterial blooms [28–31]. Quantifying the temporal and spatial dynamics of water surface temperature (WST) is therefore essential to anticipate stratification and mixing patterns, assess vulnerability to water-quality deterioration and harmful algal blooms, and guide more effective lake management to enhance water security under ongoing climate change.

This study focuses on the temporal evolution of water surface temperature (WST) in Lake Paranoá, a tropical urban reservoir, central Brazil, over a 40-year period (1984–2024). By integrating in situ measurements with remote sensing data, we aim to identify key drivers of WST variability and contribute to improved lake management strategies in the face of environmental change. The specific objectives of this work are to: (1) construct a consistent, four-decade WST time series from Landsat 5, 8, and 9 data validated with in situ observations; (2) quantify long-term trends in WST and compare them with concurrent changes in meteorological forcings; (3) examine the influence of solar radiation, air tem-

perature, relative humidity, precipitation, wind speed, evaporation, and inflows on WST at multiple temporal scales; and (4) discuss implications for lake management in tropical urban environments under climate change.

## 2. Materials and Methods

The methodological framework integrates remote sensing data and in situ measurements to analyze long-term variations in water surface temperature (WST) and their relationship with external meteorological and hydrological drivers over a 40-year period (1984–2024). The approach includes (i) the acquisition and processing of satellite imagery from Landsat missions, (ii) the compilation of ground-based observations of WST and meteorological variables, (iii) the calibration and validation of WST estimation models, and (iv) the application of statistical analyses to assess trends and correlations at multiple temporal scales (Figure 1).

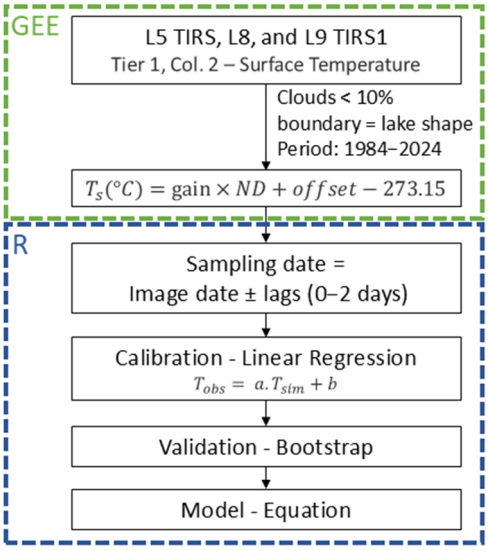


**Figure 1.** Flowchart of the methods used to obtain an equation for estimating surface temperature.

### *2.1. Study Area: Paranoá Lake, a Tropical Urban Reservoir*

Paranoá Lake is an artificial reservoir located in Brasília, Federal District, Brazil, at an elevation of approximately 1000 m (Figure 2). It drains a watershed of 1034.07 km$^2$ and is characterized by a tropical savannah climate (Aw, Köppen classification). The lake serves multiple purposes, including public water supply, hydroelectricity, fishing, navigation, recreation, and effluent dilution. It has an average depth of 12.42 m, a maximum depth of 38 m, a maximum width of 5 km, and a length of 40 km. The estimated hydraulic residence time is approximately 299 days [32–34].

Paranoá is a dendritic, compartmentalized, and warm monomitic lake in its deepest regions, with seasonal regimes of mixing and thermal–chemical stratification. These processes regulate the vertical distribution of chlorophyll-a, phytoplankton, zooplankton, dissolved oxygen (DO), and nutrients [30,33,35–38].

Situated within Brazil's capital, Paranoá is an urban lake bordered by densely populated neighborhoods, with over 500,000 inhabitants in its immediate surroundings. It receives treated effluents from two major wastewater treatment plants—the Northern and Southern WWTPs—and contains an important abstraction point for public water supply, located in the Northern Water Treatment Plant, managed by the regional sanitation authority. The lake also plays a key role in providing recreational space and thermal comfort for the urban population, highlighting its socio-environmental relevance [30]. During the 2016–2017 water crisis, Paranoá Lake was used as an emergency source of drinking water,

which emphasized its strategic role in regional water security. Concurrently, the lake experienced eutrophication events due to high nutrient loads, resulting in intense cyanobacterial blooms that posed risks to both ecosystem integrity and public health [28,30,34,38].

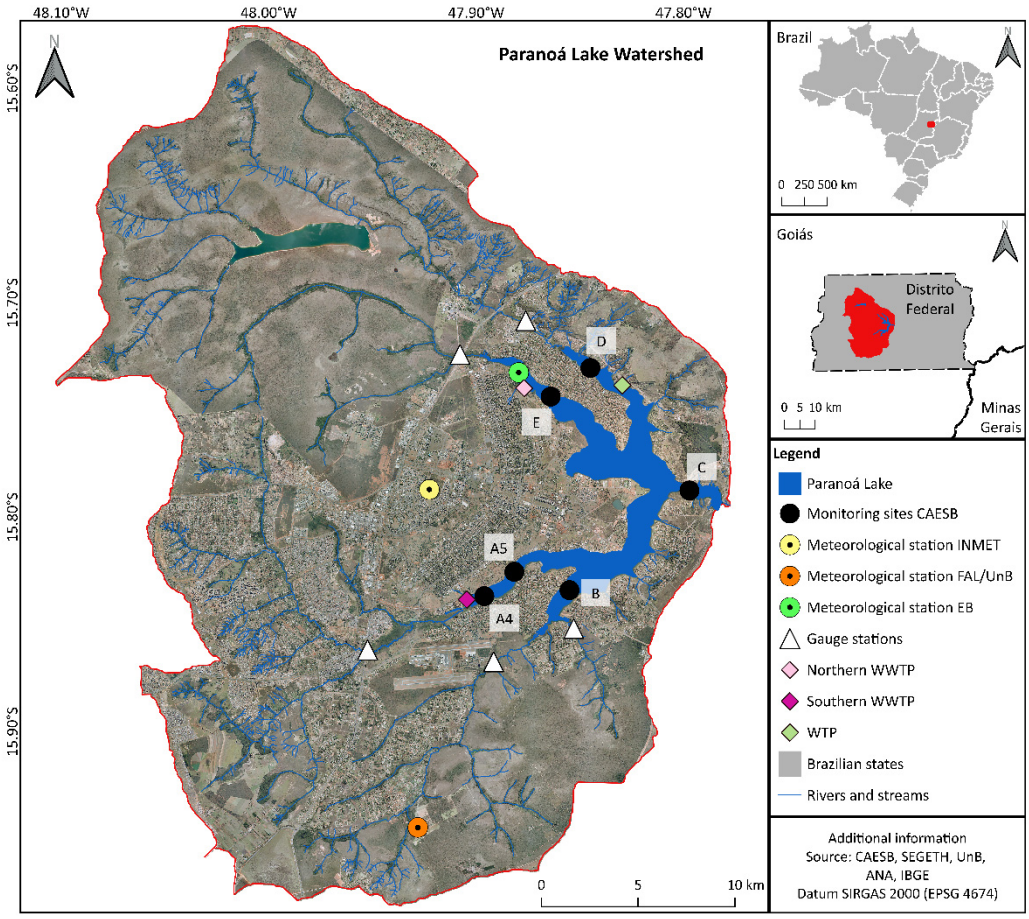


**Figure 2.** Map of Paranoá lake basin and monitoring sites' location.

### *2.2. Ground-Based Monitoring of WST, Meteorological and Hydrological Variables*

The in situ dataset includes monthly water surface temperature (WST) measurements at 1 m depth, along with meteorological and hydrological variables. WST monitoring has been conducted by CAESB (Environmental Sanitation Company of the Federal District) since 1985 at six representative locations—A4, A5, B, C, D, and E—distributed across the main branches of Lake Paranoá (Figure 2). Descriptive statistics of the WST recorded at each monitoring site are presented in Table S1 in the Supplementary Materials.

Meteorological data were obtained from the Brasília station (code 83377; yellow dot in map—Figure 2), operated by the Brazilian National Institute of Meteorology (INMET), which provides long-term hourly time series of air temperature, relative humidity, wind speed, and precipitation, as well as daily insolation data. Shortwave radiation was estimated from insolation using the Angström–Prescott equation, coefficients a = 0.282 and b = 0.490, calibrated by [39] for Brasília, Federal District, Brazil, being representative for the study area ($R^2$ of 0.93 and standard error of estimate, 1.52 MJ $m^{-2}$ $day^{-1}$) and ensuring consistency in the radiation dataset. Although wind conditions vary around the lake due to local topographic effects [40], the Brasília station was used given the continuity and availability of its anemometric records, which is essential for the temporal consistency of trend analysis in lake–climate interactions [41].

Daily evaporation data were retrieved from two monitoring sites operated by the University of Brasília: the Experimental Biology Station (EB; green dot in map—Figure 2)

with data from 1972 to 1996, and the Fazenda Água Limpa station (FAL; orange dot in map—Figure 2) with data from 2000 to 2024. These datasets were analyzed separately, given their statistically distinct variances and the contrasting settings of the stations—EB being closer to the lake and more representative of open-water evaporation conditions. The accurate characterization of evaporation in lacustrine environments is crucial, as it plays a significant role in latent heat fluxes and thermal stability [42]. Daily and monthly inflow data were compiled from several gauging stations operated by CAESB and ANA, Southern Wastewater Treatment Plant (WWTP; pink and purple rhombuses in map—Figure 2), and tributaries such as Riacho Fundo, Cabeça de Veado, Torto, Bananal, and Gama. We used only the available discharge data, after consistency analysis; no gap-filling was performed. Details on station codes, operator, and monitoring periods are provided in the Supplementary Materials (Table S2). Additionally, bathymetric data from Aguiar et al. [43] were used qualitatively to interpret spatial patterns in WST but were not included as predictors in the regression models.

### *2.3. Water Surface Temperature Retrieval from Landsat Imagery*

Water surface temperature (WST) in Lake Paranoá was estimated for the 1984–2024 period using Tier 1 Collection 2 Level-2 imagery from Landsat 5, 8, and 9. Imagery from Landsat 7 was excluded due to striping artifacts and data gaps in the study area.

All image filtering and processing were performed in Google Earth Engine [44], where scenes were selected based on acquisition date, cloud cover (<10%), and intersection with the lake's geometry. Cloud and artifact screening used the USGS QA_PIXEL bit-mask to remove pixels flagged as Fill (bit 0), Dilated cloud (bit 1), Cirrus (bit 2; L8/L9), Cloud (bit 3), and Cloud shadow (bit 4), and QA_RADSAT to exclude radiometrically saturated pixels; a shoreline mask was applied to limit mixed-pixel effects. For each scene, surface temperature was derived from the thermal band (L5: ST_B6; L8/L9: ST_B10), converted to °C using the scene-specific multiplicative and additive factors and subtracting 273.15.

Surface temperature was extracted for six CAESB monitoring sites (A4, A5, B, C, D, and E), as well as for the entire lake area. No spatial buffers were used due to the resolution of the thermal bands (100–120 m). Extracted values were exported to R and matched with in situ data within a ±2-day interval. Linear models were calibrated and evaluated using all paired data for lags of 0, 1, and 2 days. For each lag, we fitted (i) an all-samples model and (ii) a filtered model retaining only matchups with absolute error $\leq 2$ °C. This conservative threshold was defined after systematic visual inspection showing that discrepancies absolute errors greater than 2 °C were consistently associated with residual cloud, thin haze, or mixed pixels; it follows the principle of conservative filtering in [23] and aligns with outlier-screening practices for LSWT time series [19], thereby balancing sample retention and accuracy.

The model with no lag between image and field data showed the best performance and was used to estimate WST throughout the time series.

### *2.4. Model Validation and Statistical Analysis of External Drivers*

Statistical analyses were conducted in R (version 4.4.3) and RStudio (version 2024.12.1 +563) to evaluate the performance of the WST retrieval model and to quantify the influence of external drivers on lake surface temperature at multiple temporal scales. Model calibration involved fitting linear regression models between simulated and observed WST values, using time lags of 0, 1, and 2 days between satellite overpass and in situ sampling. The best-performing model was selected based on standard metrics: coefficient of determination ($R^2$), root mean square error (RMSE), mean absolute percentage error (MAPE), and bias [19].

Validation of the selected model was performed using the bootstrap method with 3000 resamples [45], implemented via the boot package [46], which enabled internal validation without excluding data from the calibration series. Calibration and validation were conducted over the full 1984–2024 period, and only temperature estimates with absolute errors below 2.0 °C were used in model fitting to minimize the effect of residual atmospheric noise and image artifacts.

After generating the complete WST series, trend analysis was conducted using the BFAST algorithm [41,47], which decomposes time series into seasonal (St), trend (Tt), and residual (et) components, allowing the identification of structural changes and gradual trends. Statistical significance of trends was assessed through ANOVA ($p < 0.05$).

To investigate the influence of meteorological and hydrological variables on WST, Pearson correlation coefficients were calculated between WST and solar radiation, air temperature, relative humidity, wind speed, precipitation, evaporation, and inflows, across daily, monthly, seasonal (wet/dry), and annual scales. Multiple linear regression models were developed for the monthly scale, considering evaporation data from both the Experimental Biology Station (EB) and Fazenda Água Limpa (FAL), due to their different variances and proximity to the lake. Multivariate analysis was realized on monthly scale due to data availability. Results were supported by diagnostic plots and exploratory visualizations.

The outputs derived from this workflow allowed not only the reconstruction of a consistent WST time series but also a robust analysis of its temporal trends and external influences.

## 3. Results

### *3.1. Estimation and Validation of Water Surface Temperature (WST)*

In situ measurements collected by CAESB at six monitoring sites revealed a statistically significant warming trend in the water surface temperature (WST) of Lake Paranoá over the 40-year period from 1984 to 2024. The data indicates a total increase of 1.34 °C, corresponding to a mean annual warming rate of 0.033 °C/yr ($p$-value = $1.16 \times 10^{-22}$). This positive trend was consistently observed across all monitoring points (Figure 3), varying from 0.027 °C/yr (B) to 0.038 °C/yr (A5), reinforcing the spatial heterogeneity of the lake's thermal response to long-term climatic and environmental changes.

To estimate WST from satellite data, linear regression models were calibrated using Landsat-derived surface temperatures and field observations collected at 1 m depth. The models were tested with time lags of 0, 1, and 2 days between image acquisition and in situ measurements. For each lag, we fitted two models: one using all matchups and another restricted to matchups with absolute error $\leq 2$ °C—an error associated with residual cirrus and/or sunglint even after cloud masking. Figure 4 shows that the filtered models (solid lines) exhibit systematically steeper slopes indicating that residual clouds and/or sunglint in the unfiltered sets may biases simulated temperatures, overestimating them through increased reflectance. This effect intensifies at higher temperatures, where differences between fits can reach approximately 1.5 °C.

Across the 0–2-day lag models, we retained 12, 27, and 41 image matchups, respectively, after QA_PIXEL bit-mask and QA_RADSAT filter (Table 1). Filtering by $|\text{error}| \leq 2$ °C had negligible impact at 0 d (still 12 scenes) and removed only one scene at 1 d and one at 2 d. Most matchups came from Landsat 8, followed by Landsat 5 and Landsat 9. Seasonally, the sample is dominated by the dry period, reflecting greater scene viability under lower cloudiness, whereas wet-season scenes accounted for 15–20% of the total in each model. Although the 2-day lag provides the largest number of matchups, the 0-day, $|\text{error}| \leq 2$ °C configuration best represents the intended matchup condition (near-synchronous satellite–in situ observations) while minimizing contamination-driven bias

and achieved the best performance metrics among the tested lags (highest $R^2$ and lowest RMSE, Figure 4). Consequently, we adopt the 0-day filtered model for WST estimation and bias correction throughout the time series, balancing representativeness (no lag) and data quality (conservative outlier removal).

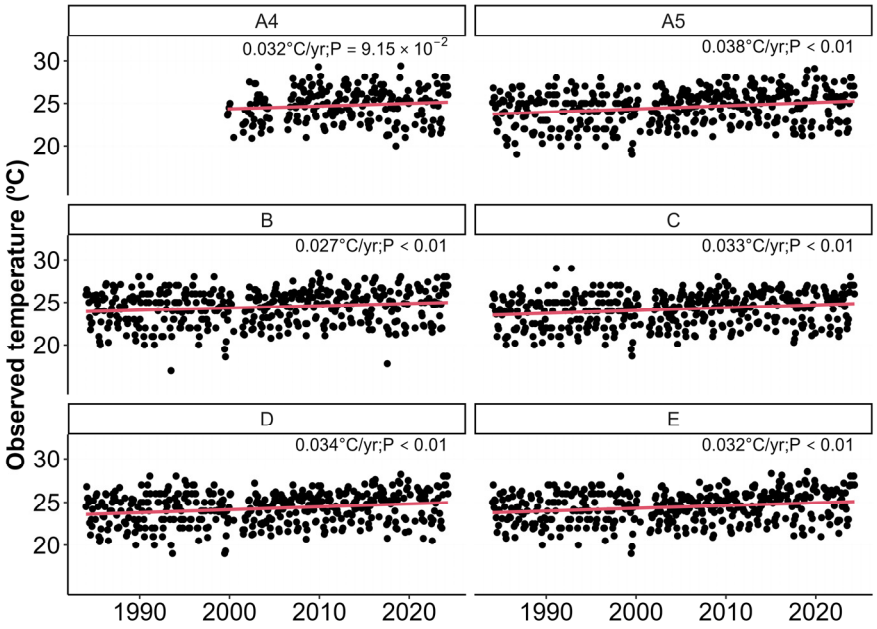


**Figure 3.** Long-term trends of observed WST at individual monitoring sites in Lake Paranoá (1984–2024). Linear regression slopes (°C $yr^{-1}$, red lines) denote warming rates.

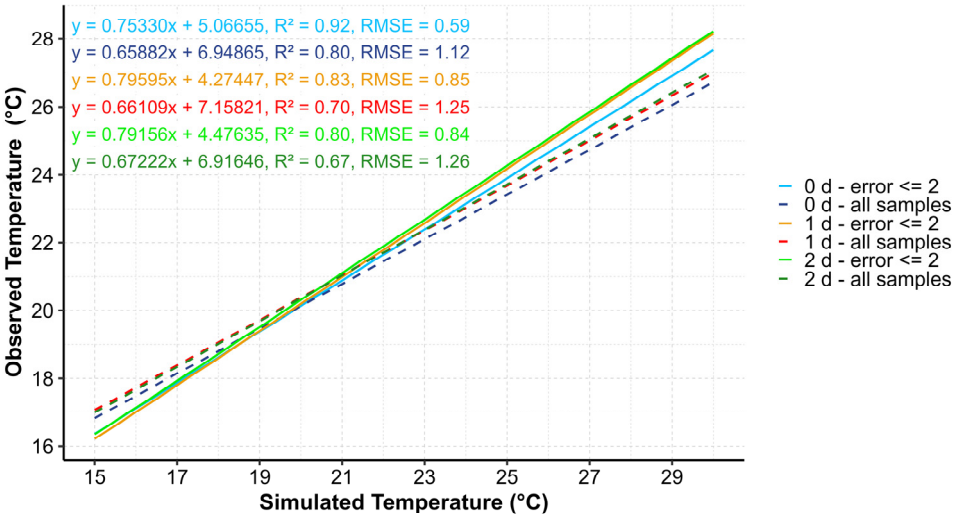


**Figure 4.** WST models under different lags (0–2 days), showing fits for all samples (dashed lines) and for matchups filtered by absolute error $\leq 2$ °C (solid lines). Divergence increases at higher temperatures and is associated with residual cloud/thin-haze and sunglint contamination in the unfiltered sets. Additional metrics, including sample size, residual standard error, bias, and MAPE, are provided in Table S3 of the Supplementary Materials.

The model using data without temporal lag (0-day) demonstrated the best performance, achieving $R^2 = 0.92$, RMSE = 0.59 °C, MAPE = 0.021, and near-zero bias (Figure 5). This configuration outperformed lagged models by approximately 0.3 °C in RMSE and was selected for simulating WST throughout the entire time series (Table S3). The best-fitting model (0-day lag) was applied to estimate the full WST time series, which served as the basis for subsequent analyses.

**Table 1.** Scene counts for WST calibration under 0–2 day lags, for all samples and for the subset with absolute error $\leq 2$ °C. Totals are stratified by sensor (Landsat 5, 8, and 9) and by season (dry and wet).

| | Number of Images | | | | | |
|---|---|---|---|---|---|---|
| | **Total** | **Landsat 5** | **Landsat 8** | **Landsat 9** | **Dry Period** | **Wet Period** |
| 0 d: all samples | 12 | 2 | 9 | 1 | 10 | 2 |
| 0 d: abs error $\leq 2$ | 12 | 2 | 9 | 1 | 10 | 2 |
| 1 d: all samples | 27 | 6 | 18 | 3 | 22 | 5 |
| 1 d: abs error $\leq 2$ | 26 | 6 | 17 | 3 | 21 | 5 |
| 2 d: all samples | 41 | 18 | 20 | 3 | 35 | 6 |
| 2 d: abs error $\leq 2$ | 40 | 18 | 19 | 3 | 34 | 6 |

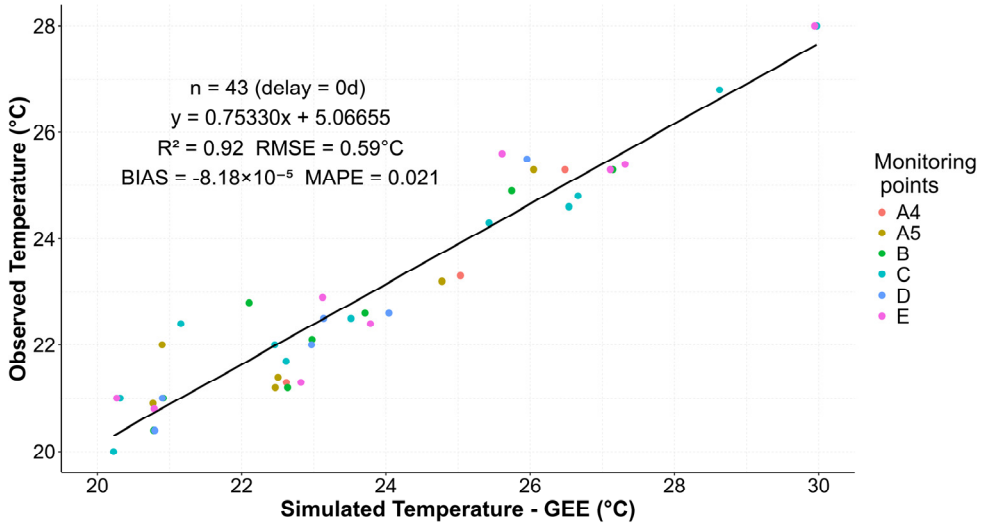


**Figure 5.** Graph of calibration ($n$ = 43) of WST Paranoá lake model for monitoring points A, B, C, D and E during 1984 to 2024 for the model with no lag (0-day delay). The black line represents the linear regression model fitted to the samples.

The adopted regression model ($WST_{estimated} = 0.75330 \times WST_{Landsat} + 5.06655$) was validated through bootstrap resampling with 3000 iterations, ensuring statistical robustness without data exclusion. The resulting 95% confidence intervals for $R^2$ (0.8513–0.9565) and RMSE (0.4950–0.7214), combined with low bias ($-0.0017$) and standard error (0.03), confirmed the model's precision and reliability in estimating lake surface temperatures across multiple decades and variable atmospheric conditions (Table 2). Simulated WST closely followed both seasonal cycles and interannual variability in the historical records, establishing a solid basis for the retrospective thermal analysis of the lake (Figure 6). It should be noted that horizontal linear patterns in the observed WST data (Figure 6) from 1990 to 1999 are probably associated with measurement errors, which may have affect both the model fit and WST estimates.

**Table 2.** Metrics and equation obtained through linear regression on validation of WST Paranoá lake model using bootstrap (adopted model: $WST_{estimated} = 0.75330 \times WST_{Landsat} + 5.06655$).

| **Metrics** | **95% Confidence Interval** | **Bias** | **Std Error** |
|---|---|---|---|
| $R^2$ | (0.8513, 0.9565) | $-1.69 \times 10^{-3}$ | 0.03 |
| RMSE | (0.4950, 0.7214) | $-1.69 \times 10^{-2}$ | 0.06 |


**Figure 6.** Time series of observed and simulated temperature (adopted model: $WST_{estimated} = 0.75330 \times WST_{Landsat} + 5.06655$).

The model was then applied to selected Landsat images to estimate the spatial distribution of WST in representative years for both the wet and dry seasons. Dates were selected based on the presence of wet–dry season imagery that maintained sufficient spatial coverage after cloud/artifact screening. The simulations for February and August of 1986, 2000, and 2023 (Figure 7) illustrate the characteristic seasonal patterns. For 2009, images from March and July are presented, since during 2009–2015 period no year provided suitable scenes for both February and August.

During the dry season, surface temperature gradients aligned with the lake's bathymetry [43]: deeper regions exhibited lower WST, while shallower branches consistently showed higher temperatures [48–50]. In contrast, wet-season distributions revealed more spatially variable isothermal patterns. Notably, Landsat 5 TM images from 1986, 2000, and 2009 were affected by radiometric noise, limiting the accurate plotting of isotherms and potentially affecting spatial consistency.

Additional spatial analyses based on selected images revealed localized thermal anomalies, particularly in branch A, where linear structures such as bridges appeared to coincide with elevated WST during the wet season. Spatial instability in isotherms was more pronounced in wet-season images from 2023, likely influenced by atmospheric interference such as thin haze, cirrus clouds, or sunglint, no rainfall was recorded on the image acquisition date or during the preceding four days. Wind conditions recorded during image acquisition suggest low-speed, southeastward flows, which support the interpretation of minimal wind-induced surface variability. A detailed account of spatial patterns and in situ measurements of wind conditions (2023 year) is provided in Figure 7.

### *3.2. Temporal Trends in Water Surface Temperature and External Forcings*

Monthly variability patterns (Figure 8) reveal distinct seasonal signals and differing statistical behaviors among variables. WST presents low interquartile dispersion and limited extreme values, suggesting strong thermal inertia and seasonal stability across the 40-year record. In contrast, air temperature exhibits wider distribution and more frequent outliers, while relative humidity displays a left-skewed pattern, typical of Brasília's semi-humid tropical climate.

Trend analysis using the BFAST algorithm allowed decomposition of each time series into seasonal, trend, and residual components (Figures S1–S9). Statistically significant positive trends were detected in WST ($\beta = 0.02$, $p = 8.17 \times 10^{-13}$), air temperature ($\beta = 0.016$, $p = 0.00$), and solar radiation ($\beta = 0.02$, $p = 0.001$), indicating an increase in both thermal input and lake temperature over time. Conversely, decreasing trends were identified for

wind speed, relative humidity, evaporation (FAL station), and stream inflows, highlighting potential long-term shifts in atmospheric and hydrological dynamics.

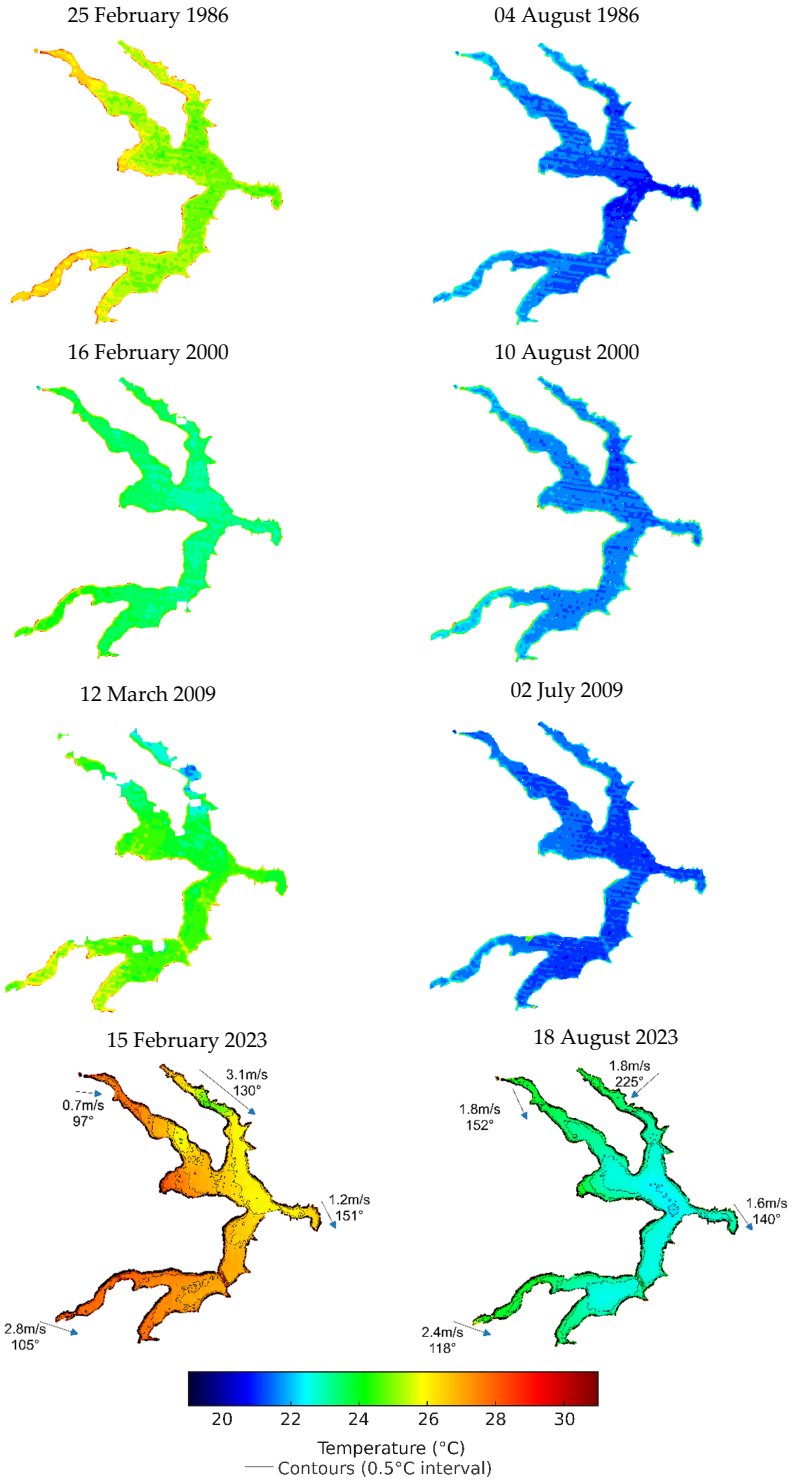


**Figure 7.** Simulated spatial distribution of water surface temperature (WST) in Lake Paranoá for wet season (February or March) and dry season (July or August) of 1986, 2000, 2009, and 2023, using the calibrated Landsat-based regression model (0-day lag). Dates were selected based on the availability of wet–dry season scenes that retained adequate spatial coverage after masking. Thermal patterns highlight seasonal variation, with warmer temperatures in shallower branches during the dry season. Radiometric noise affected the 1986, 2000, and 2009 images (Landsat 5 TM), and localized thermal anomalies were observed near bridge structures in branch A during February 2023. Blue arrows indicate the magnitude and direction of wind vectors.

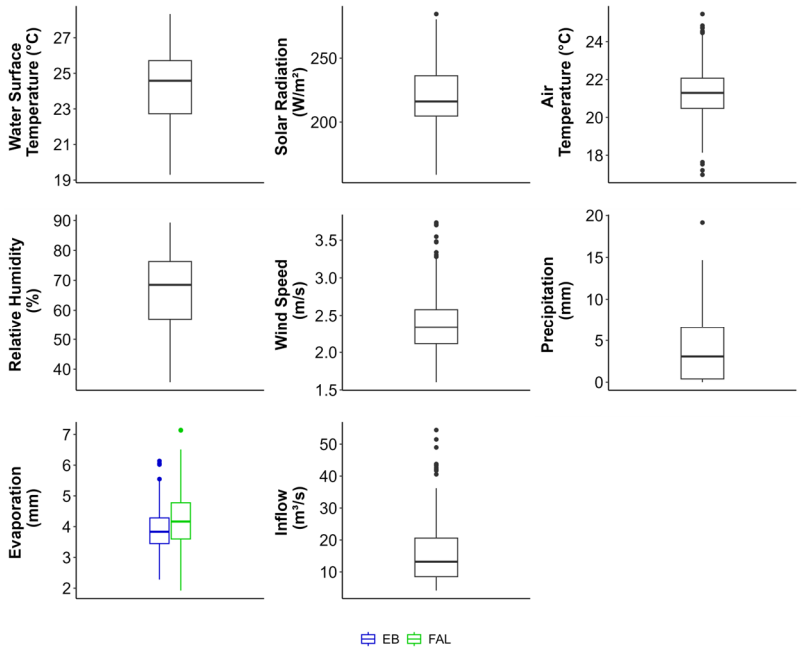


**Figure 8.** Monthly boxplot of water surface temperature (WST), solar radiation, air temperature, relative humidity, wind speed, precipitation, evaporation (EB and FAL stations), and inflow. The boxes indicate the interquartile range with the median.

Evaporation datasets from the EB and FAL stations show notably different behaviors. The EB series, monitored near the lake at 1003 m, reflects lake evaporation more directly, while the FAL series, collected at 1080 m over vegetated terrain, reflects soil-vegetation evapotranspiration. These differences are evident in their monthly distribution and trend components and justify the separate treatment of both datasets in later modeling efforts.

Sudden peaks in variables such as wind speed, rainfall, and inflows are preserved in the analysis and may reflect episodic meteorological or hydrological disturbances. For inflows, although an overall decreasing trend was observed, sharp positive anomalies occurred, likely linked to isolated storm events or basin-specific pulses. The progressive increase in solar radiation suggests higher surface energy availability, which, together with air temperature, likely contributes to the observed WST trend.

The combination of distribution patterns and temporal trends outlined in Figure 8 provides a statistical foundation for interpreting WST behavior across multiple scales. These results offer essential context for correlation and regression analyses, particularly at the monthly scale where meteorological variability most closely aligns with the satellite-derived WST dataset used in this study.

### *3.3. Multiscale Correlation Analysis Between WST and External Forcings*

On a monthly time scale, the main drivers of variation in the lake's average water surface temperature (WST) are air temperature ($R^2 = 0.43$, $p < 0.01$), relative humidity ($R^2 = 0.28$, $p < 0.01$), and wind speed ($R^2 = 0.23$, $p < 0.01$). Statistically significant positive correlations ($p < 0.05$) were also identified between WST and solar radiation, precipitation, and inflow. These relationships are detailed in the correlation matrix provided, which highlights the dominant role of atmospheric drivers in modulating WST at this temporal resolution (Figure 9).

The distribution of correlation values across variables emphasizes a consistent pattern in which air temperature exerts a positive control on WST, while wind speed is negatively associated, reflecting its role in inducing surface cooling and vertical mixing. This contrast is especially evident in periods of reduced atmospheric instability, such as the dry

season, when air temperature and wind speed present stronger correlations with WST ($R^2$ = 0.51 and $R^2$ = 0.42, respectively) than during the wet season. At an annual resolution, both variables continue to dominate the correlation structure, maintaining values above $R^2$ = 0.45. Correlation results at daily, seasonal, and annual resolutions are presented in the Supplementary Materials (Figures S10–S13).

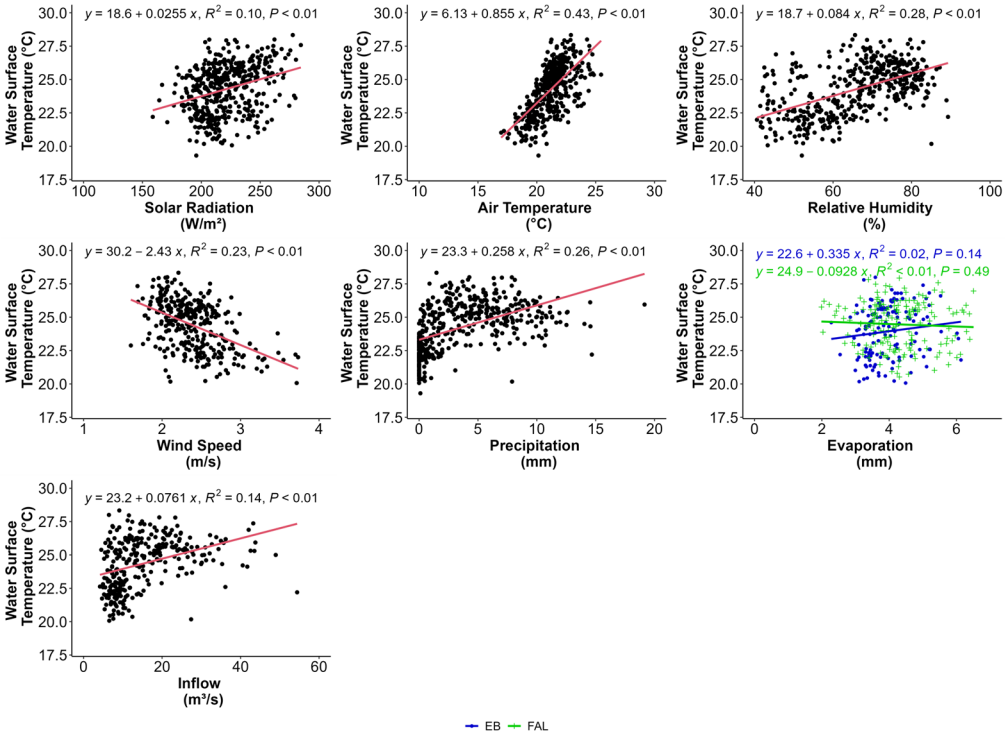


**Figure 9.** Simple Correlation between external forcings and Water Surface Temperature on a monthly scale. Linear regressions (red, blue, and green lines) represent the relationship between the analyzed variables.

Graphical results support these findings and reveal that, although other variables such as precipitation and evaporation contribute to thermal variation, their correlations with WST are notably weaker or inconsistent. A dedicated analysis considering only non-zero precipitation values further reduced $R^2$ values (Figure S14), confirming the limited explanatory power of rainfall in this context. Similarly, evaporation—whether measured at the EB or FAL stations—did not display any statistically significant linear relationship with WST at any temporal scale.

These complementary analyses reinforce the interpretation that WST dynamics in Lake Paranoá are most directly modulated by atmospheric temperature and wind-induced turbulence. The monthly results serve as the central basis for subsequent regression modeling, given their statistical strength and compatibility with the temporal resolution of the satellite-derived dataset.

### *3.4. Key Drivers of Water Surface Temperature Across Temporal Scales*

Multiple linear regression models were developed using monthly-averaged data to quantify the combined influence of meteorological and hydrological variables on the water surface temperature (WST) of Lake Paranoá. Two separate models were constructed, each incorporating solar radiation, air temperature, relative humidity, precipitation, and wind speed, but differing in the evaporation dataset used: one model included evaporation data from the EB station, and the other from the FAL station. Complete regression results are presented in Tables S4–S7 (Supplementary Materials).

The model incorporating evaporation from the EB station yielded an adjusted $R^2$ of 0.64 and a standard residual error of 1.16. In this configuration, solar radiation, air temperature, and relative humidity were the only variables that significantly contributed to explaining WST variability. Their removal from the model resulted in decreased explanatory power (reduced $R^2$) and increased residual error, indicating their central role in modulating surface thermal behavior. By contrast, precipitation, wind speed, and EB evaporation did not show statistically significant effects ($p \geq 0.48$), and their exclusion produced negligible changes in model performance.

The alternative model using FAL station evaporation achieved a stronger fit, with an adjusted $R^2$ of 0.80 and a residual error of 0.76. This improvement reflects greater internal consistency among the predictors and a closer statistical alignment with observed WST patterns. As in the previous model, solar radiation, air temperature, and relative humidity emerged as the only significant predictors. Precipitation, wind speed, evaporation, and inflow did not contribute meaningfully and were statistically non-significant ($p > 0.05$).

Together, the two models indicate that, at the monthly scale, WST in Lake Paranoá is primarily driven by atmospheric variables directly linked to energy and moisture exchange: solar radiation, air temperature, and relative humidity. The consistent lack of significance for other variables across both models suggests that, for predictive purposes at this resolution, the inclusion of additional hydrological drivers such as evaporation and inflow is unnecessary. These findings support the use of simplified atmospheric models in thermal forecasting applications, particularly in urban tropical lake systems where data availability may be limited.

## 4. Discussion

The water surface temperature (WST) is a critical indicator of climate variability and a key driver of physical and biogeochemical processes in lakes [14]. In urban tropical reservoirs, where anthropogenic and climatic pressures converge, understanding WST dynamics is essential for the management of aquatic environments as it can be used to understand and predict periods of stratification and mixing, cyanobacterial growth and blooms [8,51]. WST is an important parameter used in the study and modeling of the energy balance, hydrological cycle, evapotranspiration, physical, chemical and biological processes because it is closely correlated with the processes occurring at the water–atmosphere interface, and as an indicator of climate change [14].

Lakes' hydrodynamics, and hence WST, are the result of combined effects of external factors. Depending on local characteristics, there may be dominant forces that seasonally drive hydrodynamic processes [52,53]. Based on these understandings, this study analyzed four decades of WST in Lake Paranoá using remote sensing and in situ data, demonstrating the effectiveness of satellite imagery to detect long-term warming trends and to identify the key external forcings [8,54].

### *4.1. Water Surface Temperature and External Forcings*

The remote estimation of WST using Landsat thermal imagery proved accurate and consistent with findings from other tropical systems [19,55]. The calibration model based on a zero-day lag between satellite acquisition and field data yielded high agreement ($R^2 = 0.92$; RMSE = 0.59 °C), validating its applicability for long-term thermal monitoring. No spatial buffers were applied due to the thermal bands' native resolution (100–120 m), which already integrates temperature over a broad area. Scenes with atmospheric artifacts, such as thin clouds or sunglint, were filtered to enhance accuracy [56,57]. The use of Google Earth Engine for automated processing and the application of bootstrapping (3000 resamples) added statistical robustness [45]. These procedures enabled the construction of a 40-year

historical WST dataset with sufficient spatiotemporal resolution to capture seasonal and long-term variability.

A significant warming trend of 0.036 °C/yr was identified for Lake Paranoá, following the global trends. Notably, WST in Lake Paranoá is rising faster than air temperature (0.026 °C/yr), aligned with findings in other urban and eutrophic lakes [3,58]. Some studies showed WST warming trends which ranged from 0.012 °C/yr to 0.083 °C/yr [2,3,6,58–60]. Huang et al. [3] simulated 91 large lakes in China to assess their warming trends. 84% of the lakes showed an increasing trend, in the order of 0.053 °C/yr. Air temperature, downward longwave radiation and wind speed changes were the forces that most affected the water surface temperature. Given the combined effect of these forces on WST, the authors observed that approximately 42% of these lakes have their surface temperature rising faster than the air temperature, which was also observed by Schneider et al. [58] for six lakes in California. Sobrino et al. [2] evaluated the warming trends of the 10 largest lakes in the world, located in Asia, America, and Africa, which ranged from 0.012 °C/yr to 0.083 °C/yr. Coats et al. [59] observed a warming trend of 0.015 °C/yr for lake Tahoe in California.

Rising air temperatures enhance WST and promote more stable stratification [61]. In the case of Lake Paranoá, air temperature is correlated with the increase in the lake's average water surface temperature (WST) across all analyzed time scales (daily, monthly, wet season, dry season, and annual). However, during the wet season, this influence weakens. This phenomenon is likely due to increased cloud cover and reduced direct solar radiation, which in turn lead to lower air temperatures; the larger inflow volume increases the lake's thermal capacity, causing it to respond more slowly to variations in air temperature; more frequent and intense rainfall, as well as surface runoff, which contribute to cooling the lake's surface; wind, rainfall, and inflows that enhance water turbulence and circulation, promoting a more uniform temperature distribution.

Relative humidity plays a key role in regulating secondary processes, such as latent heat fluxes/evaporation; in other words, it does not provide energy directly to the lake [62,63]. Therefore, observed seasonal increase in relative humidity may be associated with a reduction in the evaporative cooling of the lake, reinforcing stratification [42,64,65].

Increasing solar radiation and declining wind speed also contributed to thermal accumulation and stability in the lake. A reduction in wind speed of approximately 0.48 m/s between 2000 and 2024 may indicate the presence of the "terrestrial stilling" phenomenon, reported in various mid-latitude and tropical regions [66,67]. Reductions on the order of 0.3 m/s have been reported and associated with increased surface roughness, rising aerosol emissions [66–68], and with urbanization [69–71]. Wind stilling may lead to stronger thermal stratifications by weakening air–water turbulent exchange and reducing sensible and latent heat losses, thereby enhancing surface heat retention [72], this mechanism is consistent with the increasing seasonal influence of wind detected. Therefore, a more detailed investigation of the wind speed time series is recommended to assess and further characterize the occurrence and drivers, including the rising urbanization in Paranoá lake basin, of this phenomenon in Brasília.

Wind's contribution to WST increases with time scale, becoming the most influential driver on the annual scale ($R^2$ = 0.49). Wind induces turbulence and vertical circulation, mixing water layers. While on short time scales this mixing may be negligible or masked by other factors, its cumulative effect becomes clearer over monthly and annual periods. During the dry season, wind's influence intensifies, due to higher solar input, stronger thermal gradients, lower humidity (enhancing evaporation), and reduced inflows (decreasing thermal buffering). These conditions allow wind to act more effectively on lake dynamics.

Also, it is well known that wind speed and direction fields are not uniform in space and time [40,73–75]. Therefore, the continuous action of wind over the different branches of

the lake can generate differentiated horizontal and vertical circulation patterns, distribute heat and affect the WST of the lake. In this context, it is essential to study the relation between WST and the wind speed in every branch of lake Paranoá since they have distinct hydrodynamic behaviors and are influenced by different wind speed fields [32,40].

The low correlations found, or the absence thereof, for precipitation, evaporation, and inflow may also indicate the spatial or temporal variability of the analyzed variable in relation to WST, since in this study the analyses were conducted using average values for the entire lake. Therefore, it is essential to continue monitoring WST in the lake through conventional in situ measurements, as well as by using satellite imagery and remote sensing techniques to assess the spatial variability of WST and the effects of these variables on each branch of the lake separately.

Overall, the multiscale analysis confirmed that air temperature, solar radiation, and relative humidity are the dominant drivers of WST. Air temperature showed the strongest correlations at monthly and annual scales, while wind speed exerted a more seasonal influence, particularly in the dry season [61]. Relative humidity modulated latent heat exchange, reinforcing the effects of temperature and radiation [13,42]. Although precipitation, evaporation, and inflows showed statistical significance in some tests, they did not emerge as robust predictors. These variables may influence WST locally or episodically, and their weak correlation may reflect spatial decoupling between measurement locations and WST response zones [76].

Multiple linear regression models confirmed the importance of atmospheric drivers. The best-performing model (adjusted $R^2 = 0.80$) included solar radiation, air temperature, and relative humidity as significant predictors. Wind speed and hydrological variables were not retained due to lack of statistical significance, likely due to collinearity or spatial heterogeneity [10]. These findings support the use of simplified models for thermal prediction in urban tropical lakes, especially when aiming to inform management and modeling tools.

From a physical perspective, the lake surface energy balance is governed by radiative components—shortwave radiation (SW) and longwave radiation (LW)—and by turbulent fluxes of latent heat (LE) and sensible heat (H). The seasonality and variability of these fluxes directly control stratification, mixing, and therefore the evolution of WST. Increases in SW and LW raise the net heat gain, whereas LE and H—governed by air humidity/temperature gradients and wind speed—act as the main pathways of energy loss [5,12,77].

In this manuscript, the correlations between WST and meteorological variables (air temperature, relative humidity, wind speed, and SW derived from insolation) can be interpreted as proxies for evaluating the lake's energy balance. In summary, SW captures radiative input; cloud cover (implicit in SW variability) modulates LW; air temperature represents H; and wind and relative humidity regulate LE.

Our results align with the expected sign and seasonality of the governing fluxes, and the literature indicates that LE often dominates the cooling budget, especially during dry and windy periods, whereas net radiation explains most of the warming at seasonal scales [5,14,78]. Under conditions of low relative humidity and increased wind speed—typical of the dry season in the region—turbulent losses via latent heat flux (LE) increase, which favors cooling of the surface layer and weakens the stratification. LE is a dominant cooling pathway whose magnitude increases with wind speed and vapor-pressure deficit (i.e., low relative humidity), while H depends on the air–water temperature gradient [10,22,79].

### *4.2. Limitations*

Some limitations were noted, included: (i) sparse calibration points and gaps in the image dataset; (ii) the use of spatially averaged WST values; (iii) meteorological data were obtained from off-lake stations; and (iv) atmospheric interference in thermal remote sensing.

Irregular satellite acquisition dates and the limited number of in situ–satellite matchups used to calibrate the WST retrieval can reduce representativeness, particularly during the summer (wet season). Beyond sample size, uneven sampling intervals and gaps may also affect both the BFAST decomposition and the correlation analyses with external forcings, introducing noise to the estimated trend and seasonal components, affecting breakpoint detection and biasing seasonal amplitude [80]. Scenes concentrated in the dry season can reduce the robustness of correlations with meteorological and hydrological drivers by biasing the strength of statistical associations.

In the wet period, when air and water temperatures are typically higher, the calibration set provides fewer observations, which may weaken the model's ability to characterize temporal variability and degrade performance under warm conditions. This issue is especially relevant for the 1990s, when episodes of eutrophication likely elevated WST [81–83], yet the scarcity of usable scenes constrained calibration, thereby limiting the robustness of the retrieval. Accordingly, we acknowledge limitations in the model's performance with respect to seasonality and eutrophication processes, owing to temporal gaps arising from irregular spacing between viable images, monthly-scale observation intervals, and missing data within the time series.

The temperature series (observed + simulated) was filled in by considering the images selected through visual inspection. Images containing cloud interference, especially cirrus clouds and sunglint that were not captured by the quality band and/or cloud filter, and patterns similar to those associated with high errors in model calibration were manually removed and disregarded.

The estimation of surface temperature involves several problems and limitations: (i) estimating emissivity is complex and involves uncertainties due to spectral heterogeneities, including in water bodies; (ii) atmospheric interference affects the estimation of the received radiance; (iii) masks may fail to detect all atmospheric interferences, such as thin haze and cirrus clouds, resulting in pixels with residual interference; and (iv) orbital variations may cause the sunglint effect [56,57].

In addition, the resampling of Landsat 5, 8 and 9 imagery can introduce artificial spatial detail and increase the likelihood of mixed pixels, especially along shorelines or in small water bodies, potentially biasing temperature estimates. In order to avoid the edge effect and the sampling of an extensive area, no buffer was used in the data acquisition of the selected points.

The analysis was carried out considering the mean surface temperature of the lake, so the influences discussed in the results refer to average changes in the lake. However, the lake has different characteristics per compartment (arms and central) and therefore receives and responds differently to external forcings depending on the compartment. It is therefore important that, when a larger time series of observed WST is available for each compartment, these analyses should be carried out by arm of Lake Paranoá.

It is important to note that variables such as evaporation, precipitation, and inflow exhibit greater spatial variability. As a result, their relationship with water surface temperature (WST) may not be fully captured in the present analyses, which are based on spatially average data. The influence of these variables may act more locally or at specific locations within the lake.

Inflows from WWTP effluents and tributaries can exert localized control on WST. Effluent discharges are typically warmer than lake water and generate surface thermal

plumes, whereas tributaries often contribute cooler water. In Lake Paranoá, for example, conditions in the Riacho Fundo arm reflect the combined influence of the WWTP outfall and the tributary input, favoring greater thermal stability and thus stronger stratification. In this context, purely statistical regressions are challenging, owing to collinearity among drivers, shoreline mixed pixels at thermal resolution, and nonlinear advection/stratification processes. A more robust approach is to pair branch-specific inflow records (Riacho Fundo) with co-located observed temperatures to test their interrelationships and to simulate the separate and joint effects of each source using 3D hydrodynamic modeling.

Additionally, the available observed variables analyzed were measured at a greater distance from the lake, which may have influenced the analysis and the correlations. For example: Brasilia is characterized by convective rainfall, so the rainfall measured at the INMET station may not represent the rainfall over Lake Paranoá, thus affecting the correlation between WST and rainfall.

Beyond local meteorology, large-scale climate modes (e.g., ENSO and the SAMS/SACZ), which are not addressed in this study, drive interannual variability by altering cloudiness, humidity, and wind regimes over central Brazil, thereby modifying the radiative and the turbulent heat fluxes at the lake surface. Such climate linkages imply that interannual changes in WST can partly reflect remotely forced anomalies in radiative and turbulent fluxes [84]. Incorporating these modes would improve the attribution of WST variability to specific climate drivers.

We emphasize that the meteorological variables used here function as proxies for heat-flux terms, not direct flux measurements. This has implications: (i) the heat budget is not explicitly closed; (ii) irregular image dates and seasonal sampling bias (greater dry-season coverage) may over-represent radiative control and under-represent advective terms; and (iv) collinearity among predictors (e.g., air temperature, downward longwave radiation, and humidity) limits causal separation. Accordingly, correlations should be read as physically consistent evidence, rather than quantitative partitioning of fluxes.

The applied technique is replicable in other urban settings; however, because the model is empirical, it requires site-specific calibration with in situ measurements, as the simulated–observed relationship depends on each lake's thermal variability. Extrapolating the model to other urban lakes should therefore be undertaken with caution. The physical mechanisms underlying these relationships—energy exchange at the air–water interface, and modulation of stratification stability—are generalizable across lakes sharing similar climatic regimes, morphometry, and anthropogenic pressures. Thus, while the methodological framework and process-based inferences are applicable to other tropical urban reservoirs, WST model parameters must be calibrated locally [5,7,9].

Despite these challenges, the results support the integration of satellite-derived WST into hydrodynamic and water quality models, particularly for simulating stratification, mixing, and oxygen dynamics under changing climatic conditions [85–88]. Continued monitoring and refined modeling efforts at sub-basin scale are recommended to enhance predictive capacity and support water management strategies.

### *4.3. Management Implications and Future Perspectives*

Remote sensing data, such as water surface temperature (WST), can be integrated with other datasets, such as meteorological data, for use in numerical modeling, e.g., hydrodynamic, watershed, and water quality models. Both water surface temperature and external forcing variables are essential components for modeling processes [89].

The retrieval of WST through remote sensing in water bodies with large spatial extent and thermal variability, such as Lake Paranoá, combined with in situ measurements, enables

broader spatial and temporal coverage, facilitating the detection and analysis of thermal patterns, trends, seasonal variations, and extreme events [90].

WST is intrinsically linked to thermal and chemical stratification, internal circulation, gas solubility, and biogeochemical processes, making it a key variable in hydrodynamic and water quality modeling. Understanding how WST responds to the external forcings, how it affects the dynamics of the aquatic ecosystem, and how this information can be implemented in mathematical modeling enhances the diagnostic, predictive, and forecasting capabilities, especially when considering climate change and water resource management contexts [86,87].

High-resolution satellite-derived WST data can improve the spatial accuracy of simulations by reducing discrepancies between observation scales and model grid resolution. Also, estimated WST data can be employed as spatially distributed initial conditions for temperature across the entire lake, as well as for calibration and validation of hydrodynamic and water quality models [85–88].

The identification of air temperature, solar radiation, and relative humidity as the primary drivers of WST variability provides an actionable basis for reservoir management in Lake Paranoá. Integrating high-resolution meteorological forecasts into hydrodynamic and water quality models can allow short-term predictions of stratification events and guide preventive measures such as artificial mixing or withdrawal.

The observed long-term warming trend suggests that nutrient load thresholds may require revision to mitigate the risk of harmful algal blooms under warmer conditions. The progressive reduction in wind speed may require site-specific circulation interventions in deeper branches to prevent hypolimnetic anoxia.

Spatial heterogeneity in WST also highlights the importance of branch-specific monitoring, informing localized measures. Incorporating routine remote sensing-based WST monitoring into decision-making frameworks would enable near-real-time detection of atypical warming events, supporting faster and more effective responses.

Future perspectives, given this study's findings and limitations, include:

- Improve automation and reproducibility of WST retrievals by defining and implementing a lake-specific atmospheric-correction strategy for cirrus clouds and sunglint.
- Acquiring water temperature and meteorological data closer to the lake and, where necessary, at higher temporal frequency, enabling analysis of external forcings on both the central basin and the individual branches.
- Quantify the surface heat budget and large-scale climate drivers: compute and validate the main air–water heat-flux components, net shortwave and longwave radiation, sensible and latent heat fluxes, to better represent air–water energy exchange. In parallel, incorporate larger-scale climate factors (e.g., ENSO/ONI, PDO, AMO) to contextualize interannual–decadal variability and extremes.
- Examining heat-budget variables—sensible heat flux, latent heat flux, and longwave radiation— to improve the predictive skill of WST models.
- Integrating satellite-derived temperature fields into 3D hydrodynamic and ecological models to simulate stratification dynamics, nutrient cycling, and algal/cyanobacterial blooms under different climate and land-use/land-cover scenarios, as well as to test potential management interventions (e.g., artificial mixing or withdrawal).
- Assimilate satellite-derived WST into 3D hydrodynamic model to quantify the contributions of external forcings—including heat fluxes—to WST variability and long-term trends.

## 5. Conclusions

This study aimed to analyze the influence of external forcings (meteorological and inflow) on the average water surface temperature (WST) of Lake Paranoá. The estimation of WST using imagery from Landsat 5, 8, and 9 satellites enabled the construction of a historical time series with greater spatial and temporal coverage, revealing well-defined seasonal patterns and a warming trend over recent decades. Landsat 7 scenes were excluded because striping artifacts and coverage gaps over the lake that compromised data quality and continuity.

The observed warming trend of average WST in the lake (0.036 °C/yr) is higher than that of air temperature (0.026 °C/yr), reflecting the impact of global warming. The main external forcings found to be correlated with WST were air temperature, wind speed, relative humidity, and solar radiation. At shorter time scales, such as daily and monthly, air temperature, wind speed, and relative humidity showed significant correlations with changes in average WST. On monthly and seasonal scales, air temperature and wind presented significant correlations; on an annual scale, wind stood out as the most influential factor due to its continuous action.

The analysis also revealed a decreasing trend in wind speed since 2000, which may be contributing to the intensification of thermal stratification in the lake. Stronger stratification may limit turbulence and vertical mixing, negatively affecting water quality.

Although statistically significant correlations were identified, the $R^2$ values found were generally moderate. This may be partly explained by the use of lake-wide average WST values, which may have masked more localized spatial variations across the different branches of Lake Paranoá, each of which exhibits distinct hydrodynamic behaviors.

This context highlights the importance of continuing WST monitoring—both conventional and through remote sensing—and of subsequently analyzing the correlations between external forcings and WST for each compartment of the lake. The integration of these datasets with numerical modeling will enhance the understanding of the lake's hydrodynamic and biogeochemical processes, as well as strengthen predictive and management capabilities in the face of climate change.

Considering the limitations of the present study, future perspectives and suggestions include:

i. improving automation and reproducibility of WST retrieval processes;
ii. defining a strategy and implementing atmospheric correction for cirrus clouds and sunglint over the lake to automate the estimation process;
iii. analyzing wind influence on lake thermal dynamics by incorporating additional descriptors such as fetch length, wind direction, persistence, and spatial heterogeneity of wind fields;
iv. expanding data acquisition and monitoring to evaluate these relationships between variables within each lake branch.

**Supplementary Materials:** The following supporting information can be downloaded at: https://www.mdpi.com/article/10.3390/rs17213603/s1, Table S1. Descriptive statistics (mean, standard deviation, minimum, maximum, and interquartile range) of the water surface temperature (WST) recorded at each monitoring site (A4, A5, B, C, D, and E) and for the daily lakewide average. Results are presented separately for the wet and dry seasons, as well as for the full time series (1984–2024). Table S2. Monitoring variables used in this study, including frequency, observation stations, responsible operators, and periods of data availability. The dataset integrates meteorological, hydrological, and limnological parameters used for modeling and statistical analyses of water surface temperature (WST) in Lake Paranoá from 1984 to 2024. Table S3. Tested models with 0, 1 and 2 day delay, with absolute errors lower than 2 and all samples. Table S4. Multiple regression model results assessing the influence of meteorological and hydrological variables on WST at monthly scale. Table

S5. Model including EB evaporation (coefficients, *p*-values, and diagnostics). Table S6. Multiple regression model results assessing the influence of meteorological and hydrological variables on WST at monthly scale. Table S7. Model including FAL evaporation (coefficients, *p*-values, and diagnostics). Figure S1. Monthly water surface temperature time series (Yt), seasonal component (St), trend component (Tt), and error component (et). Figure S2. Monthly solar radiation time series (Yt), seasonal component (St), trend component (Tt), and error component (et). Figure S3. Monthly air temperature time series (Yt), seasonal component (St), trend component (Tt), and error component (et). Figure S4. Monthly relative humidity time series (Yt), seasonal component (St), trend component (Tt), and error component (et). Figure S5. Monthly wind speed time series (Yt), seasonal component (St), trend component (Tt), and error component (et). Records for 1991–2000 were excluded due to data inconsistencies. Figure S6. Monthly precipitation time series (Yt), seasonal component (St), trend component (Tt), and error component (et). Figure S7. Monthly evaporation on EB station time series (Yt), seasonal component (St), trend component (Tt), and error component (et). Figure S8. Monthly evaporation on FAL station time series (Yt), seasonal component (St), trend component (Tt), and error component (et). Figure S9. Monthly inflow time series (Yt), seasonal component (St), trend component (Tt), and error component (et). Figure S10. Simple correlations between WST and external forcings (solar radiation, air temperature, relative humidity, precipitation, wind speed, evaporation, and inflow) at a daily time scale. The matrix highlights the reduced explanatory power of individual variables at this resolution. Figure S11. Correlation analysis between WST and external forcings during the wet season. Wind speed and air temperature show the strongest associations, though with lower $R^2$ values compared to the dry season. Figure S12. Correlation analysis between WST and external forcings during the dry season. Air temperature and wind speed are the dominant predictors of WST under dry and stable atmospheric conditions. Figure S13. Correlation analysis between WST and external forcings at the annual scale. Air temperature and wind speed remain the most influential drivers of long-term variability in WST. Figure S14. Simple correlation—Monthly: precipitation vs. precipitation > 0.

**Author Contributions:** Conceptualization, A.R.P., T.d.A., R.E.C. and S.K.; methodology, A.R.P., T.d.A., R.E.C. and S.K.; software, A.R.P. and A.d.A.; validation, A.R.P. and A.d.A.; formal analysis, A.R.P. and A.d.A.; data curation, A.R.P. and A.d.A.; writing—original draft preparation, A.R.P.; writing—review and editing, A.R.P., T.d.A., R.E.C. and S.K.; visualization, A.R.P. and A.d.A.; supervision, R.E.C. and S.K.; project administration, R.E.C. and S.K.; funding acquisition, S.K. All authors have read and agreed to the published version of the manuscript.

**Funding:** This research was funded by CNPq (Conselho Nacional de Desenvolvimento Científico e Tecnológico) grant number 160714/2021-4, FAP-DF (Fundação de Apoio à Pesquisa do Distrito Federal) grant numbers 0193.000721/2016, 00193-00000286/2023-71, and 0193.00001264/2025-91, CAPES (Coordenação de Aperfeiçoamento de Pessoal de Nível Superior)/ANA (Agência Nacional de Águas e Saneamento Básico) 88887.115882/2015-01, Decanato de Pesquisa e Inovação (DPI) and the Biblioteca Central (BCE) of the Universidade de Brasília (UnB) through Call No. 001/2025 DPI/BCE/UnB. This research was supported by the PDI 002/2023 Project (CAESB/ADASA/UnB).

**Data Availability Statement:** Data are available on request. Script for water surface temperature retrieval: https://code.earthengine.google.com/3f72307bbee5ba1258e6019e5ef731a3 (accessed on 1 July 2025).

**Acknowledgments:** The authors would like to thank CAESB (Companhia de Saneamento Ambiental do Distrito Federal) for kindly providing hydrological data and water surface temperature from lake Paranoá within the scope of the research and innovation program PDI 002 Caesb/Adasa in partnership with the University of Brasília (UnB). We also acknowledge ANA (Agência Nacional de Águas e Saneamento Básico) for providing hydrological data, INMET (Instituto Nacional de Meteorologia) for meteorological data, and UnB for providing evaporation data. The authors further acknowledge financial support from CNPq, FAP-DF, ANA CAPES, PDI 002 Project (CAESB/ADASA/UnB), DPG/UnB, and DPI/UnB.

**Conflicts of Interest:** The authors declare no conflicts of interest.

## Abbreviations

The following abbreviations are used in this manuscript:

| | |
|---|---|
| WWTP | Wastewater Treatment Plant |
| WTP | Water Treatment Plant |
| WST | Water Surface Temperature |
| FAL | Fazenda Água Limpa (location of an evaporation monitoring site) |
| EB | Estação da Biologia (location of an evaporation monitoring site) |
| INMET | National Institute of Meteorology (Instituto Nacional de Meteorologia) |
| CAESB | Environmental Sanitation Company of Federal District (Companhia de Saneamento Ambiental do Distrito Federal) |
| GEE | Google Earth Engine |
| ANA | Water National Agency (Agência Nacional de Águas) |
| UnB | University of Brasília |
| SW | Shortwave Radiation |
| LW | Longwave Radiation |
| LH | Latent Heat |
| H | Sensible Heat |
| ENSO | El Niño-Southern Oscillation |
| ONI | Oceanic Niño Index |
| PDO | Pacific Decadal Oscillation |
| AMO | Atlantic Multi-decadal Oscillation |
| SAMS | South American Monsoon System |
| SACZ | South Atlantic Convergence Zone |

## References

1. Wang, X.; Shi, K.; Zhang, Y.; Qin, B.; Zhang, Y.; Wang, W.; Woolway, R.I.; Piao, S.; Jeppesen, E. Climate Change Drives Rapid Warming and Increasing Heatwaves of Lakes. *Sci. Bull.* **2023**, *68*, 1574–1584. [CrossRef]
2. Sobrino, J.A.; García-Monteiro, S.; Julien, Y. An Analysis of the Lake Surface Water Temperature Evolution of the World's Largest Lakes during the Years 2003–2020 Using MODIS Data. *Recent Adv. Remote Sens.* **2024**, *1*, 1–9. [CrossRef]
3. Huang, L.; Woolway, R.I.; Timmermann, A.; Lee, S.-S.; Rodgers, K.B.; Yamaguchi, R. Emergence of Lake Conditions That Exceed Natural Temperature Variability. *Nat. Geosci.* **2024**, *17*, 763–769. [CrossRef]
4. Dorjsuren, B.; Zemtsov, V.A.; Batsaikhan, N.; Demberel, O.; Yan, D.; Hongfei, Z.; Yadamjav, O.; Chonokhuu, S.; Enkhbold, A.; Ganzorig, B.; et al. Trend Analysis of Hydro-Climatic Variables in the Great Lakes Depression Region of Mongolia. *J. Water Clim. Change* **2024**, *15*, 940–957. [CrossRef]
5. Woolway, R.I.; Merchant, C.J. Worldwide Alteration of Lake Mixing Regimes in Response to Climate Change. *Nat. Geosci.* **2019**, *12*, 271–276. [CrossRef]
6. Song, S.; Yang, J.; Liu, L.; Bai, G.; Zhou, J.; McKay, D. Lake Surface Water Temperature in China from 2001 to 2021 Based on GEE and HANTS. *Ecol. Inform.* **2024**, *84*, 102903. [CrossRef]
7. O'Reilly, C.M.; Sharma, S.; Gray, D.K.; Hampton, S.E.; Read, J.S.; Rowley, R.J.; Schneider, P.; Lenters, J.D.; McIntyre, P.B.; Kraemer, B.M.; et al. Rapid and Highly Variable Warming of Lake Surface Waters around the Globe. *Geophys. Res. Lett.* **2015**, *42*, 10773–10781. [CrossRef]
8. Jiang, Y.; Guo, C.; Su, F.; Xu, W.; Ma, L.; Cui, L.; Mi, C. Climate Warming Effects on Temperature Structure in Lentic Waters: A Bibliometric Analysis from the Recent 20 Years. *Ecol. Indic.* **2024**, *167*, 112740. [CrossRef]
9. Zhou, J.; Leavitt, P.R.; Rose, K.C.; Wang, X.; Zhang, Y.; Shi, K.; Qin, B. Controls of Thermal Response of Temperate Lakes to Atmospheric Warming. *Nat. Commun.* **2023**, *14*, 6503. [CrossRef]
10. Tong, Y.; Feng, L.; Wang, X.; Pi, X.; Xu, W.; Woolway, R.I. Global Lakes Are Warming Slower than Surface Air Temperature Due to Accelerated Evaporation. *Nat. Water* **2023**, *1*, 929–940. [CrossRef]
11. Jia, T.; Yang, K.; Peng, Z.; Tang, L.; Duan, H.; Luo, Y. Review on the Change Trend, Attribution Analysis, Retrieval, Simulation, and Prediction of Lake Surface Water Temperature. *IEEE J. Sel. Top. Appl. Earth Obs. Remote Sens.* **2022**, *15*, 6324–6355. [CrossRef]
12. Bouffard, D.; Kiefer, I.; Wüest, A.; Wunderle, S.; Odermatt, D. Are Surface Temperature and Chlorophyll in a Large Deep Lake Related? An Analysis Based on Satellite Observations in Synergy with Hydrodynamic Modelling and in-Situ Data. *Remote Sens. Environ.* **2018**, *209*, 510–523. [CrossRef]

13. Liu, C.; Wang, S.; Liu, X.; Zhou, H.; Li, B.; Du, Y.; Wang, L. Characteristics of Water Quality Response to Hypolimnetic Anoxia in Daheiting Reservoir. *Water Sci. Technol.* **2022**, *85*, 2065–2075. [CrossRef] [PubMed]
14. Winton, R.S.; Calamita, E.; Wehrli, B. Reviews and Syntheses: Dams, Water Quality and Tropical Reservoir Stratification. *Biogeosciences* **2019**, *16*, 1657–1671. [CrossRef]
15. Elçi, Ş. Effects of Thermal Stratification and Mixing on Reservoir Water Quality. *Limnology* **2008**, *9*, 135–142. [CrossRef]
16. Greb, S.; Dekker, A.; Binding, C. (Eds.) *Earth Observations in Support of Global Water Quality Monitoring*; IOCCG Report Series, No. 17; International Ocean Colour Coordinating Group: Dartmouth, NS, Canada, 2018; ISBN 978-1-896246-67-3.
17. Mishra, D.R.; Ogashawara, I.; Gitelson, A.A. (Eds.) *Bio-Optical Modelling and Remote Sensing of Inland Waters*; Elsevier: Amsterdam, The Netherlands, 2017; ISBN 978-0-12-804644-9.
18. Gholizadeh, M.; Melesse, A.; Reddi, L. A Comprehensive Review on Water Quality Parameters Estimation Using Remote Sensing Techniques. *Sensors* **2016**, *16*, 1298. [CrossRef] [PubMed]
19. Pedreros-Guarda, M.; Abarca-del-Río, R.; Escalona, K.; García, I.; Parra, Ó. A Google Earth Engine Application to Retrieve Long-Term Surface Temperature for Small Lakes. Case: San Pedro Lagoons, Chile. *Remote Sens.* **2021**, *13*, 4544. [CrossRef]
20. Vijayakumar, S.; Saravanakumar, R.; Arulanandam, M.; Ilakkiya, S. Google Earth Engine: Empowering Developing Countries with Large-Scale Geospatial Data Analysis—A Comprehensive Review. *Arab. J. Geosci.* **2024**, *17*, 139. [CrossRef]
21. Zhao, Q.; Yu, L.; Li, X.; Peng, D.; Zhang, Y.; Gong, P. Progress and Trends in the Application of Google Earth and Google Earth Engine. *Remote Sens.* **2021**, *13*, 3778. [CrossRef]
22. Woolway, R.I.; Kraemer, B.M.; Lenters, J.D.; Merchant, C.J.; O'Reilly, C.M.; Sharma, S. Global Lake Responses to Climate Change. *Nat. Rev. Earth Environ.* **2020**, *1*, 388–403. [CrossRef]
23. Vanhellemont, Q. Automated Water Surface Temperature Retrieval from Landsat 8/TIRS. *Remote Sens. Environ.* **2020**, *237*, 111518. [CrossRef]
24. Desgué-Itier, O.; Melo Vieira Soares, L.; Anneville, O.; Bouffard, D.; Chanudet, V.; Danis, P.A.; Domaizon, I.; Guillard, J.; Mazure, T.; Sharaf, N.; et al. Past and Future Climate Change Effects on the Thermal Regime and Oxygen Solubility of Four Peri-Alpine Lakes. *Hydrol. Earth Syst. Sci.* **2023**, *27*, 837–859. [CrossRef]
25. Adrian, R.; O'Reilly, C.M.; Zagarese, H.; Baines, S.B.; Hessen, D.O.; Keller, W.; Livingstone, D.M.; Sommaruga, R.; Straile, D.; Van Donk, E.; et al. Lakes as Sentinels of Climate Change. *Limnol. Oceanogr.* **2009**, *54*, 2283–2297. [CrossRef] [PubMed]
26. Ren, L.; Liu, Y.; Lauridsen, T.L.; Søndergaard, M.; Han, B.; Wang, J.; Jeppesen, E.; Zhou, J.; Wu, Q.L. Warming Exacerbates the Impact of Nutrient Enrichment on Microbial Functional Potentials Important to the Nutrient Cycling in Shallow Lake Mesocosms. *Limnol. Oceanogr.* **2021**, *66*, 2481–2495. [CrossRef]
27. Yang, K.; Yu, Z.; Luo, Y.; Yang, Y.; Zhao, L.; Zhou, X. Spatial and Temporal Variations in the Relationship between Lake Water Surface Temperatures and Water Quality—A Case Study of Dianchi Lake. *Sci. Total Environ.* **2018**, *624*, 859–871. [CrossRef]
28. Brostel, R.; Mühlhofer, S.I.; Serique, E.F.S.; Starling, F.L.R.M.; Oliveira, L.S.; Borges, M.N.; de Lima, T.G. *Caesb Inova—Crise Hídrica: Superação em Tempo Recorde*; Companhia de Saneamento Ambiental do Distrito Federal (Caesb): Brasilia, Brazil, 2018; p. 48.
29. Angelini, R.; Bini, L.M.; Starling, F.L.R.M. Efeitos de Diferentes Intervenções no Processo de Eutrofização do Lago Paranoá (BRASÍLIA-DF). *Oecol. Austr.* **2008**, *12*, 564–571. [CrossRef]
30. Mar Da Costa, N.Y.; Boaventura, G.R.; Mulholland, D.S.; Araújo, D.F.; Moreira, R.C.A.; Faial, K.C.F.; Bomfim, E.D.O. Biogeochemical Mechanisms Controlling Trophic State and Micropollutant Concentrations in a Tropical Artificial Lake. *Environ. Earth Sci.* **2016**, *75*, 854. [CrossRef]
31. Padovesi-Fonseca, C.; Philomeno, M.G. Effects of Algicide (Copper Sulfate) Application on Short-Term Fluctuations of Phytoplankton in Lake Paranoá, Central Brazil. *Braz. J. Biol.* **2004**, *64*, 819–826. [CrossRef]
32. Nunes, G.; Minoti, R.T.; Koide, S. Mathematical Modeling of Watersheds as a Subsidy for Reservoir Water Balance Determination: The Case of Paranoá Lake, Federal District, Brazil. *Hydrology* **2020**, *7*, 85. [CrossRef]
33. Batista, B.D.; Fonseca, B.M. Fitoplâncton Da Região Central Do Lago Paranoá (DF): Uma Abordagem Ecológica e Sanitária. *Eng. Sanit. Ambient.* **2018**, *23*, 229–241. [CrossRef]
34. Da Silva, D.B.; Bellotto, V.R.; Barbosa, J.D.S.B.; Lima, T.B. Spatiotemporal Variation on Water Quality and Trophic State of a Tropical Urban Reservoir: A Case Study of the Lake Paranoá-DF, Brazil. *Water* **2021**, *13*, 3314. [CrossRef]
35. Pinto-Coelho, R.M. Flutuações sazonais e de curta duração na comunidade zooplanctônica do lago Paranoá, Brasília-DF, Brasil. *Rev. Brasil. Biol.* **1987**, *47*, 17–29.
36. Batista, C.A. Estrutura da Comunidade Zooplanctônica e Qualidade da água no Lago Paranoá, Brasília-DF. Master's Thesis, Universidade de Brasília, Brasília-DF, Brazil, 2007.
37. Fernandes, T.D.S.; Gomes, L.N.L. Avaliação do Comportamento de Parâmetros Limnológicos de Qualidade da água na Região mais Profunda do Lago Paranoá/DF. XIV Encontro Nacional de Estudantes de Engenharia Ambiental, Brasília, Brazil. *Blucher Eng. Proc.* **2016**, *3*, 334–340. [CrossRef]
38. Barbosa, C.C.; Gomes, L.N.L.; Minoti, R.T. A Modelling Approach to Simulate Chlorophyta and Cyanobacteria Biomasses Based on Historical Data of a Brazilian Urban Reservoir. *Rev. Ambiente Água* **2021**, *16*, 1–11. [CrossRef]

39. Dornelas, K.D.E.S.; Silva, C.L.D.; Oliveira, C.A.D.S. Coeficientes Médios da Equação de Angström-Prescott, Radiação Solar e Evapotranspiração de Referência em Brasília. *Pesq. Agropec. Bras.* **2006**, *41*, 1213–1219. [CrossRef]
40. Pereira, A.R.; Argenta, T.S.; Cicerelli, R.E.; Koide, S. A Variabilidade do Evento em Agosto e Dezembro de 2021 às Margens do Lago Paranoá, Brasília-DF, Brasil. In Proceedings of the Anais do 32° Congresso da ABES, Belo Horizonte, Brazil, 21–24 May 2023.
41. Verbesselt, J.; Hyndman, R.; Newnham, G.; Culvenor, D. Detecting Trend and Seasonal Changes in Satellite Image Time Series. *Remote Sens. Environ.* **2010**, *114*, 106–115. [CrossRef]
42. Schmid, M.; Hunziker, S.; Wüest, A. Lake Surface Temperatures in a Changing Climate: A Global Sensitivity Analysis. *Clim. Change* **2014**, *124*, 301–315. [CrossRef]
43. Aguiar, A.C.N.; Ianniruberto, M.; Borges, W.R.; Roig, H.L.; Turquetti, G.N.; de França, P.H.P. *Mapeamento Topo-Batimétrico de Reservatório Utilizando LIDAR e Batimetria no Lago Paranoá-DF*; Sociedade Brasileira de Geofísica (SBGf): Rio de Janeiro, Brazil, 2019.
44. Gorelick, N.; Hancher, M.; Dixon, M.; Ilyushchenko, S.; Thau, D.; Moore, R. Google Earth Engine: Planetary-Scale Geospatial Analysis for Everyone. *Remote Sens. Environ.* **2017**, *202*, 18–27. [CrossRef]
45. Davison, A.C.; Hinkley, D.V. *Bootstrap Methods and Their Application*, 1st ed.; Cambridge University Press: Cambridge, UK, 1997; ISBN 978-0-521-57391-7.
46. Canty, A.; Ripley, B.D. Boot: Bootstrap R (S-Plus) Functions 2024. Available online: https://10.32614/CRAN.package.boot (accessed on 7 August 2024).
47. Verbesselt, J.; Hyndman, R.; Zeileis, A.; Culvenor, D. Phenological Change Detection While Accounting for Abrupt and Gradual Trends in Satellite Image Time Series. *Remote Sens. Environ.* **2010**, *114*, 2970–2980. [CrossRef]
48. Skowron, R. Thermal Structure of Water During the Summer in Lakes of the Polish Lowlands as a Result of Their Varied Morphometry. *Limnol. Rev.* **2020**, *20*, 89–95. [CrossRef]
49. Boehrer, B.; Schultze, M. Stratification of Lakes. *Rev. Geophys.* **2008**, *46*, 2006RG000210. [CrossRef]
50. Herb, W.R.; Stefan, H.G. Temperature Stratification and Mixing Dynamics in a Shallow Lake with Submersed Macrophytes. *Lake Reserv. Manag.* **2004**, *20*, 296–308. [CrossRef]
51. Qin, B.; Deng, J.; Shi, K.; Wang, J.; Brookes, J.; Zhou, J.; Zhang, Y.; Zhu, G.; Paerl, H.W.; Wu, L. Extreme Climate Anomalies Enhancing Cyanobacterial Blooms in Eutrophic Lake Taihu, China. *Water Resour. Res.* **2021**, *57*, e2020WR029371. [CrossRef]
52. Son, J.Y.; Han, H.J.; Cho, Y.-C.; Kang, T.; Im, J.K. Seasonal Variations in the Thermal Stratification Responses and Water Quality of the Paldang Lake. *Water* **2024**, *16*, 3057. [CrossRef]
53. Olsson, F.; Mackay, E.B.; Spears, B.M.; Barker, P.; Jones, I.D. Interacting Impacts of Hydrological Changes and Air Temperature Warming on Lake Temperatures Highlight the Potential for Adaptive Management. *Ambio* **2025**, *54*, 402–415. [CrossRef]
54. Bhateria, R.; Jain, D. Water Quality Assessment of Lake Water: A Review. *Sustain. Water Resour. Manag.* **2016**, *2*, 161–173. [CrossRef]
55. Lamaro, A.A.; Mariñelarena, A.; Torrusio, S.E.; Sala, S.E. Water Surface Temperature Estimation from Landsat 7 ETM+ Thermal Infrared Data Using the Generalized Single-Channel Method: Case Study of Embalse Del Río Tercero (Córdoba, Argentina). *Adv. Space Res.* **2013**, *51*, 492–500. [CrossRef]
56. Li, Z.-L.; Tang, B.-H.; Wu, H.; Ren, H.; Yan, G.; Wan, Z.; Trigo, I.F.; Sobrino, J.A. Satellite-Derived Land Surface Temperature: Current Status and Perspectives. *Remote Sens. Environ.* **2013**, *131*, 14–37. [CrossRef]
57. Shi, K.; Han, J.-C.; Wang, P. Near Real-Time Retrieval of Lake Surface Water Temperature Using Himawari-8 Satellite Imagery and Machine Learning Techniques: A Case Study in the Yangtze River Basin. *Front. Environ. Sci.* **2024**, *11*, 1335725. [CrossRef]
58. Schneider, P.; Hook, S.J.; Radocinski, R.G.; Corlett, G.K.; Hulley, G.C.; Schladow, S.G.; Steissberg, T.E. Satellite Observations Indicate Rapid Warming Trend for Lakes in California and Nevada. *Geophys. Res. Lett.* **2009**, *36*, 2009GL040846. [CrossRef]
59. Coats, R.; Perez-Losada, J.; Schladow, G.; Richards, R.; Goldman, C. The Warming of Lake Tahoe. *Clim. Change* **2006**, *76*, 121–148. [CrossRef]
60. Brkić, Ž. Increasing Water Temperature of the Largest Freshwater Lake on the Mediterranean Islands as an Indicator of Global Warming. *Heliyon* **2023**, *9*, e19248. [CrossRef]
61. Wang, Y.; Li, Y.; Cheng, Y.; Wang, Y.; Zhu, Y.; Li, R.; Acharya, K.; Ibrahim, M. Thermal Stratification and Mixing Processes Response to Meteorological Factors in a Monomictic Reservoir. *J. Environ. Manag.* **2024**, *354*, 120205. [CrossRef]
62. Brutsaert, W. *Evaporation into the Atmosphere*; Springer: Dordrecht, The Netherlands, 1982; ISBN 978-90-481-8365-4.
63. Shuttleworth, W.J. *Terrestrial Hydrometeorology*; Wiley-Blackwell: Hoboken, NJ, USA, 2012; ISBN 978-0-470-65937-3.
64. Li, Z.; Zhang, Z.; Xiong, S.; Zhang, W.; Li, R. Lake Surface Temperature Predictions under Different Climate Scenarios with Machine Learning Methods: A Case Study of Qinghai Lake and Hulun Lake, China. *Remote Sens.* **2024**, *16*, 3220. [CrossRef]
65. Liu, Z.; Yang, H.; Li, C.; Wang, T. Estimating the Sensitivity of the Priestley–Taylor Coefficient to Air Temperature and Humidity. *Hydrol. Earth Syst. Sci.* **2024**, *28*, 4349–4360. [CrossRef]
66. Bichet, A.; Wild, M.; Folini, D.; Schär, C. Causes for Decadal Variations of Wind Speed over Land: Sensitivity Studies with a Global Climate Model. *Geophys. Res. Lett.* **2012**, *39*, 2012GL051685. [CrossRef]

67. Zhang, Z.; Wang, K.; Chen, D.; Li, J.; Dickinson, R. Increase in Surface Friction Dominates the Observed Surface Wind Speed Decline during 1973–2014 in the Northern Hemisphere Lands. *J. Clim.* **2019**, *32*, 7421–7435. [CrossRef]
68. Deng, K.; Liu, W.; Azorin-Molina, C.; Yang, S.; Li, H.; Zhang, G.; Minola, L.; Chen, D. Terrestrial Stilling Projected to Continue in the Northern Hemisphere Mid-Latitudes. *Earth's Future* **2022**, *10*, e2021EF002448. [CrossRef]
69. Chen, X.; Jeong, S.; Park, H.; Kim, J.; Park, C.-R. Urbanization Has Stronger Impacts than Regional Climate Change on Wind Stilling: A Lesson from South Korea. *Environ. Res. Lett.* **2020**, *15*, 054016. [CrossRef]
70. Wang, J.; Feng, J.; Yan, Z.; Zha, J. Urbanization Impact on Regional Wind Stilling: A Modeling Study in the Beijing-Tianjin-Hebei Region of China. *JGR Atmos.* **2020**, *125*, e2020JD033132. [CrossRef]
71. Hou, A.; Ni, G.; Yang, H.; Lei, Z. Numerical Analysis on the Contribution of Urbanization to Wind Stilling: An Example over the Greater Beijing Metropolitan Area. *J. Appl. Meteorol. Climatol.* **2013**, *52*, 1105–1115. [CrossRef]
72. Woolway, R.I.; Meinson, P.; Nõges, P.; Jones, I.D.; Laas, A. Atmospheric Stilling Leads to Prolonged Thermal Stratification in a Large Shallow Polymictic Lake. *Clim. Change* **2017**, *141*, 759–773. [CrossRef]
73. Potisomporn, P.; Vogel, C.R. Spatial and Temporal Variability Characteristics of Offshore Wind Energy in the United Kingdom. *Wind Energy* **2022**, *25*, 537–552. [CrossRef]
74. Morais, G.M.D.; Sobrinho, J.E.; Santos, W.D.O.; Costa, D.D.O.; Silva, S.T.A.D.; Maniçoba, R.M. Caracterização Da Velocidade e Direção Do Vento Em Mossoró/RN (Characterization of Wind Speed and Direction in Mossoró/RN). *Rev. Bras. Geog. Fis.* **2014**, *7*, 746–754. [CrossRef]
75. Maggiotto, S.R.; Ferreira, F.M.; Maximiano, C.V. Um Estudo da Velocidade e Direção Predominante do Vento em Brasília, DF. In Proceedings of the XVIII Congresso Brasileiro de Agrometeorologia—XVIII CBA 2013 and VII Reunião Latino Americana de Agrometeorologia, Belém, PA, Brazil, 16–19 September 2013.
76. Stefaniak, O.M.; Fitzpatrick, F.A.; Dow, B.A.; Blount, J.D.; Sullivan, D.J.; Reneau, P.C. Influences of Meteorological Conditions, Runoff, and Bathymetry on Summer Thermal Regime of a Great Lakes Estuary. *J. Great Lakes Res.* **2024**, *50*, 102416. [CrossRef]
77. Wang, W.; Xiao, W.; Cao, C.; Gao, Z.; Hu, Z.; Liu, S.; Shen, S.; Wang, L.; Xiao, Q.; Xu, J.; et al. Temporal and Spatial Variations in Radiation and Energy Balance across a Large Freshwater Lake in China. *J. Hydrol.* **2014**, *511*, 811–824. [CrossRef]
78. Magee, M.R.; Wu, C.H. Response of Water Temperatures and Stratification to Changing Climate in Three Lakes with Different Morphometry. *Hydrol. Earth Syst. Sci.* **2017**, *21*, 6253–6274. [CrossRef]
79. Matta, E.; Amadori, M.; Free, G.; Giardino, C.; Bresciani, M. A Satellite-Based Tool for Mapping Evaporation in Inland Water Bodies: Formulation, Application, and Operational Aspects. *Remote Sens.* **2022**, *14*, 2636. [CrossRef]
80. Slater, L.; Villarini, G. On the Impact of Gaps on Trend Detection in Extreme Streamflow Time Series. *Int. J. Climatol.* **2017**, *37*, 3976–3983. [CrossRef]
81. Mei, X.; Gao, S.; Liu, Y.; Hu, J.; Razlustkij, V.; Rudstam, L.G.; Jeppesen, E.; Liu, Z.; Zhang, X. Effects of Elevated Temperature on Resources Competition of Nutrient and Light Between Benthic and Planktonic Algae. *Front. Environ. Sci.* **2022**, *10*, 908088. [CrossRef]
82. Williamson, C.E.; Overholt, E.P.; Pilla, R.M.; Leach, T.H.; Brentrup, J.A.; Knoll, L.B.; Mette, E.M.; Moeller, R.E. Ecological Consequences of Long-Term Browning in Lakes. *Sci. Rep.* **2015**, *5*, 18666. [CrossRef]
83. Pilla, R.M.; Williamson, C.E.; Zhang, J.; Smyth, R.L.; Lenters, J.D.; Brentrup, J.A.; Knoll, L.B.; Fisher, T.J. Browning-Related Decreases in Water Transparency Lead to Long-Term Increases in Surface Water Temperature and Thermal Stratification in Two Small Lakes. *JGR Biogeosci.* **2018**, *123*, 1651–1665. [CrossRef]
84. Costa, J.C.; Verdan, I.; Silva, M.E.S.; Oscar-Júnior, A.C.; Ambrizzi, T. South Atlantic Convergence Zone and ENSO Occurrence in the 2000–2021 Period. *Theor. Appl. Clim.* **2024**, *155*, 7079–7093. [CrossRef]
85. Allan, M.G.; Hamilton, D.P.; Trolle, D.; Muraoka, K.; McBride, C. Spatial Heterogeneity in Geothermally-Influenced Lakes Derived from Atmospherically Corrected Landsat Thermal Imagery and Three-Dimensional Hydrodynamic Modelling. *Int. J. Appl. Earth Obs. Geoinf.* **2016**, *50*, 106–116. [CrossRef]
86. Babbar-Sebens, M.; Li, L.; Song, K.; Xie, S. On the Use of Landsat-5 TM Satellite for Assimilating Water Temperature Observations in 3D Hydrodynamic Model of Small Inland Reservoir in Midwestern US. *Adv. Remote Sens.* **2013**, *2*, 214–227. [CrossRef]
87. Baracchini, T.; Chu, P.Y.; Šukys, J.; Lieberherr, G.; Wunderle, S.; Wüest, A.; Bouffard, D. Data Assimilation of in Situ and Satellite Remote Sensing Data to 3D Hydrodynamic Lake Models: A Case Study Using Delft3D-FLOW v4.03 and OpenDA v2.4. *Geosci. Model Dev.* **2020**, *13*, 1267–1284. [CrossRef]
88. Javaheri, A.; Babbar-Sebens, M.; Miller, R.N. From Skin to Bulk: An Adjustment Technique for Assimilation of Satellite-Derived Temperature Observations in Numerical Models of Small Inland Water Bodies. *Adv. Water Resour.* **2016**, *92*, 284–298. [CrossRef]

89. Duka, M.A.; Bernardo, T.L.B.; Casim, N.C.I.; Tamayo, L.V.Q.; Monterey, M.L.E.; Yokoyama, K. Understanding Stratification and Turnover Dynamics of a Tropical Lake Using Extensive Field Observations and 3D Hydrodynamic Simulations. *Sci. Total Environ.* **2024**, *946*, 174397. [CrossRef]
90. Kramer, G.; Filho, W.P.; De Carvalho, L.A.S.; Trindade, P.M.P.; Da Rosa, C.N.; Dezordi, R. Performance and Validation of Water Surface Temperature Estimates from Landsat 8 of the Itaipu Reservoir, State of Paraná, Brazil. *Environ. Monit. Assess.* **2023**, *195*, 137. [CrossRef]